High-resolution restoration of diffuse optical images reconstructed by the photon average trajectories method

Alexander B Konovalov[1] and Vladimir V Lyubimov[2]

[1] Russian Federal Nuclear Centre – Institute of Technical Physics, P.O. Box 245, Snezhinsk, Chelyabinsk Region, 456770 Russia
[2] Research Institute for Laser Physics, 12 Birzhevaya Lin., St.-Petersburg, 199034 Russia

E-mail: a.b.konovalov@vniitf.ru

Abstract

The possibility of improving the spatial resolution of diffuse optical images reconstructed by the photon average trajectories (PAT) method is substantiated. The PAT method recently presented by us is based on a concept of an average statistical trajectory for transfer of light energy, the photon average trajectory (PAT). The inverse problem of diffuse optical tomography (DOT) is reduced to solution of integral equation with integration along a conditional PAT. As a result the conventional algorithms of projection computed tomography can be used for fast reconstruction of diffuse optical images. In our recent works we have shown that the application of the backprojection algorithms with special filtration of shadows allows a 20%-gain in spatial resolution to be obtained. But the shortcoming of the backprojection algorithms is that they can not reconstruct accurately the object regions located close to the boundary. In the present paper we consider alternative approach to improve the spatial resolution, which may be applied to images reconstructed with the use of algebraic techniques. It is based on post-reconstruction restoration of images blurred due to averaging over spatial distributions of photons, which form the signal measured by the receiver. We suggest a spatially invariant blurring model to restore local regions of a diffuse image with the use of standard deconvolution algorithms. Two iterative non-linear algorithms: the maximum-likelihood algorithm and the Lucy-Richardson algorithm are considered. It is shown that both of them allow the spatial resolution to be improved. The effect of the improvement is identical to that obtained with the use of the backprojection algorithms.

Keywords: diffuse optical tomography, photon average trajectory, spatial resolution, spatially invariant blurring model, image deblurring, deconvolution algorithms.

1. Introduction

The main problem of medical diffuse optical tomography (DOT) is in low spatial resolution due to multiple light scattering, which causes photons to propagate diffusely in a tissue. To reconstruct diffuse optical images with best resolution 'well-designed' methods such as Newton-like and gradient-like ones [1-3], which use exact forward models, are generally applied. These methods belong to a class of so-called 'multi-step' techniques, as the weighting matrix of equation system is updated on each iteration of the solution approximation. Those require computing time not less than a few minutes for 2D image reconstruction and consequently are inapplicable for real-time medical exploration. Over the past few years we have presented a new DOT method [4-11] based on a concept of an average statistical trajectory for transfer of light energy, the photon average trajectory (PAT). By this method, the inverse problem of DOT is reduced to solution of integral equation, analog of the Radon transform with integration along a conditional PAT, which is curvilinear in the common case. As result the PAT method may be implemented as a 'one-step' technique with the use of fast algorithms of projection computed tomography and can save the reconstruction time considerably. Furthermore we have shown via numerical experiment [11-15] that new method can compete with 'well-designed' ones in reconstruction accuracy, at least, for the instance of low contrast absorbing inhomogeneity. The application of the backprojection algorithms with special filtration of shadows (Vainberg or hybrid Vainberg-Butterworth filtration [12-15]) allows a 20%-gain in spatial resolution to be obtained. But the Radon transform algorithms can reconstruct accurately only internal regions of the object, remote well away from the boundary, when the PATs are close to the straight lines. As the object surface is approached, the PATs are deflected from the straight lines due to the effect of

photon migration beyond the boundary and the image is distorted. Unlike the filtered backprojection algorithms the algebraic techniques may be applied to reconstruct the bounder regions of the object as well as the internal ones. We have shown in [11] that the algebraic techniques such as the QR-factorization least-squares algorithm [16] and the multiplicative reconstruction technique [17] allow the images of good quality without visible noise to be obtained. But the spatial resolution of these images is degree worse than that of images reconstructed with the use of the backprojection algorithms. Is there a way to improve the spatial resolution in the case, when the special filtration of shadows can not be used? The study presented is a maiden attempt to answer this question. The main idea is to apply the post-reconstruction restoration of diffuse optical images. The fact is that the PAT method reconstructs the images blurred due to averaging over spatial distributions of photons, which form the signal measured by the receiver. We will show that such blurring is spatially variant and linear inverse filtering or iterative non-linear deconvolution algorithms can not be applied for image deblurring in the strict sense. In practice the optical inhomogeneities occupy only small local regions of the object. The locations of these regions become to be known after blurred image reconstruction. We develop the spatially invariant blurring model to deblur local regions of an image, which are characterized by different displacements from the object centre. A blurred image is further expressed as convolution of an isotropic Gaussian point spread function (PSF) and an ideal underlying image. At once the PSF kernel width s differs for different regions being restored and depends on the region displacement from the object centre. To study the efficiency of the blurring model proposed, a numerical experiment on cross-sectional reconstruction of cylindrical scattering objects with absorbing inhomogeneities is conducted and two iterative non-linear deconvolution algorithms are applied for image restoration. Those are the maximum-likelihood (ML) algorithm [18-21] and the Lucy-Richardson (LR) algorithm [18, 20]. We will show below that both of them allow a good gain in spatial resolution to be achieved. In number this gain is estimated by means of the modulation transfer function (MTF) and seems to be identical to that obtained with the use of the backprojection algorithms.

2. Theoretical backgrounds

2.1 The theoretical spatial resolution of blurred image

The PAT concept is based on a probabilistic interpretation of the process of the photon energy transport from a source space-time point $(0,0)$ to a receiver space-time point $(\mathbf{r},t)$. Lyubimov *et al* [4-8] have shown that a relative contribution of photons located at an intermediate space-time point $(\mathbf{r}_1,t')$ to the value of photon density at $(\mathbf{r},t)$ can be characterized by a conditional probability density:

$$P(\mathbf{r}_1,t';\mathbf{r},t)=\frac{P(\mathbf{r}_1,t')P(\mathbf{r}-\mathbf{r}_1,t-t')}{P(\mathbf{r},t)}, \qquad (1)$$

where $P(\mathbf{r},t)$ is a probability density of the photon migration from $(0,0)$ to $(\mathbf{r},t)$. The conditional probability density $P(\mathbf{r}_1,t';\mathbf{r},t)$ can be defined analytically, for example, with the use of the diffusion approximation of light propagation. As it well known [1-3], this model is widely used in optical tomography. Let the photon density $j(\mathbf{r},t)$ satisfy the time-dependent diffusion equation for a volume V with a limited piecewise-closed smooth surface $\partial\Omega$ for an instantaneous point source and the Robin boundary condition:

$$\left[a(\mathbf{r})j(\mathbf{r},t)+b(\mathbf{r})\frac{\partial j(\mathbf{r},t)}{\partial h}\right]_{\mathbf{r}\in\partial\Omega}, \qquad (2)$$

where $\partial/\partial h$ is the derivative in the direction of the outer normal to the surface $\partial\Omega$ at the point $\mathbf{r}\in\partial\Omega$, and $a(\mathbf{r})$ and $b(\mathbf{r})$ are arbitrary functions, for which the solution of the diffusion equation in volume V is nonnegative. The probability density $P(\mathbf{r}_1,t';\mathbf{r},t)$ can be expressed [4, 6, 11] as

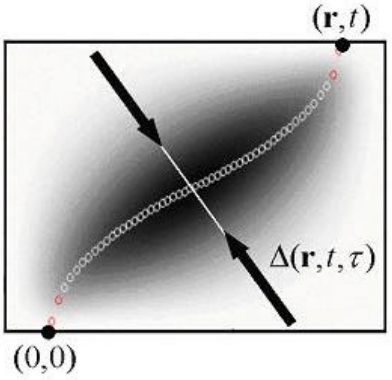

Figure 1. The effective width of the zone of the most probable trajectories for the object in the form of a flat layer. The PAT is shown by circles.

$$P(\mathbf{r}_1,t\,;\mathbf{r},t)=\frac{j\,(\mathbf{r}_1,t\,)G(\mathbf{r}-\mathbf{r}_1,t-t\,)}{\int\limits_V j\,(\mathbf{r}_1,t\,)G(\mathbf{r}-\mathbf{r}_1,t-t\,)d^3r_1}, \tag{3}$$

where $G(\mathbf{r},t)$ is the Green function. The probability density $P(\mathbf{r}_1,t\,;\mathbf{r},t)$, as a function of variable $\mathbf{r}_1$, for each fixed time value t, describes instantaneous distribution of diffuse photons. Correspondingly, the time integral $\int_0^t P(\mathbf{r}_1,x;\mathbf{r},t)dx$ for each t describes instantaneous distribution of diffuse photon trajectories. At time moment $t=t$ such distribution forms a 'banana-shaped' zone of the most probable trajectories of photons migrated from $(0,0)$ to $(\mathbf{r},t)$ (figure 1). The approximate description of this zone for a limited space V can be realized through two statistical moments:

$$\mathbf{R}(\mathbf{r},t,t\,)=\int\limits_V \mathbf{r}_1 P(\mathbf{r}_1,t\,;\mathbf{r},t)d^3r_1\,, \tag{4}$$

$$\Delta(\mathbf{r},t,t\,)=\left[\int\limits_V \left|\mathbf{r}_1-\mathbf{R}(\mathbf{r}_1,t,t\,)\right|^2 P(\mathbf{r}_1,t\,;\mathbf{r},t)d^3r_1\right]^{1/2}. \tag{5}$$

The first moment $\mathbf{R}(\mathbf{r},t,t\,)$, as a function of time t, describes the trajectory of mass centre of photon distribution. We have called it the average statistical trajectory of photon energy transfer or the photon average trajectory (PAT). Correspondingly, the second moment $\Delta(\mathbf{r},t,t\,)$ describes the standard root-mean-square deviation (RMS deviation) of photon position from the PAT and characterizes the effective width of the zone of the most probable trajectories for each time moment t (Fig. 1). Actually, as Lyubimov [5, 7] has shown, the value $\Delta(\mathbf{r},t,t\,)$ defines the theoretical spatial resolution of DOT by the PAT method. Furthermore, the RMS deviation of photons from the average trajectory depends slightly upon the object form and coincides virtually with the RMS deviation in the infinite media [8]. Therefore, to estimate the resolution for the objects of complex forms, the simple formulas for the infinite media may by used. Indeed, the well-known solution of the diffusion equation for the homogeneous infinite media with constant optical parameters: the diffusion coefficient D_0, the absorption coefficient m_{a0}, and the refraction index n_0 is written as follows

$$j_0(\mathbf{r},t) = G_0(\mathbf{r},t) = (4pD_0ct/n_0)^{-3/2} \exp\left(-\frac{|\mathbf{r}|^2 n_0}{4D_0ct} - \frac{m_{a0}ct}{n_0} \right), \tag{6}$$

where c is the light velocity in vacuum. The substitution of solution (6) into expressions (3) and (5) gives the following simple formulas for $P(\mathbf{r}_1,t;\mathbf{r},t)$ and $\Delta(\mathbf{r},t,t)$:

$$P(\mathbf{r}_1,t;\mathbf{r},t) = (\sqrt{2p}\,s)^{-3} \exp\left(-\frac{|\mathbf{r}t/t - \mathbf{r}_1|^2}{2s^2} \right), \text{ where } s = \sqrt{\frac{2D_0ct}{n_0}\left(1-\frac{t}{t}\right)} \tag{7}$$

$$\Delta(\mathbf{r},t,t) = \sqrt{12D_0c\left(t - \frac{|\mathbf{r}|n_0}{c}\right)\frac{t(t-t)}{n_0t^2}}\,. \tag{8}$$

For example, let we have a spherical or circular scattering object with diameter $d = 6.8\,cm$ and optical parameters $D_0 = 0.0636\ cm$ and $n = 1.58$. Let us assume a source and a receiver to lie on the object boundary and to be poles asunder. Then the calculation under the formulae (8) for time-gating delay $t = 600\ ps$ gives the following results: $\Delta|_{t=t/2} \approx 0.94\ cm$ and $\Delta|_{t=t/4} = \Delta|_{t=3t/4} \approx 0.81\ cm$. The first value obtained estimates the spatial resolution for the central region of the object and the second one estimates the resolution for regions remote from the center over a half radius.

2.2 On a validity of a spatially invariant blurring model

In order to use linear inverse filtering or iterative non-linear deconvolution algorithms for image restoration in the strict sense, the blurring process needs to be invariant to a spatial shift. In this case only the blurred image $\langle f \rangle$ is expressed as convolution of an isotropic PSF p and an ideal underlying image f:

$$\langle f \rangle = p \otimes f = \int_V p(\mathbf{r}_1) f(\mathbf{r}-\mathbf{r}_1) d^3r_1 = \int_V f(\mathbf{r}_1) p(\mathbf{r}-\mathbf{r}_1) d^3r_1, \tag{9}$$

where $\otimes$ is the convolution operator. Let us define a relative shadow g as a logarithm of the relation between the value of the signal intensity I caused by presence of the inhomogeneities and the value of unperturbed signal intensity I_0, measured at the object surface at the time moment t. Lyubimov *et al* [8, 10, 11] have shown that for $I_0 - I << I_0$, when the perturbation theory may be used, the relative shadow can be expressed in the form of the fundamental equation of the PAT method.

$$g(L,t) = \int_L \frac{c}{n_0 n(l)} \left(\int_V S(\mathbf{r}_1,t) P(\mathbf{r}_1,t;\mathbf{r},t)\, d^3r_1 \right) dl\,, \tag{10}$$

where L is a PAT from a source to a receiver, $n(l)$ is a velocity of the mass centre of photon distribution, which moves along the PAT, $S(\mathbf{r},t)$ is a inhomogeneity distribution function. In general case function $S(\mathbf{r},t)$ describes local disturbances $dD(\mathbf{r})$, $dm_a(\mathbf{r})$, and $dn(\mathbf{r})$ of the diffusion coefficient $D(\mathbf{r})$, the absorption coefficient $m_a(\mathbf{r})$, and the refraction index $n(\mathbf{r})$, correspondingly; and is defined by the expression [4, 5]

$$S(\mathbf{r},t) = \frac{m_{a0}dD(\mathbf{r})}{D_0} - dm_a(\mathbf{r}) + \left(\frac{n_0 dD(\mathbf{r})}{c\,D_0} - \frac{dn(\mathbf{r})}{c} \right) \frac{\partial}{\partial t} \ln j_0(\mathbf{r},t)\,. \tag{11}$$

For the practically important case of an absorbing inhomogeneity, when $dD(\mathbf{r}) = 0$ and $dn(\mathbf{r}) = 0$, function (11) takes the simple form:

$$S(\mathbf{r},t) = -d\mu_a(\mathbf{r}). \tag{12}$$

In the case of a composite absorbing and scattering inhomogenety, when $dn(\mathbf{r}) = 0$, expression (11) can be converted to a form suitable for further separation of spatial distributions $d\mu_a(\mathbf{r})$ and $dD(\mathbf{r})$:

$$S(\mathbf{r},t) \cong -d\mu_a(\mathbf{r}) + \frac{n_0^2 v^2(l)}{4c^2 D_0^2} dD(\mathbf{r}). \tag{13}$$

Using the approaches of projection tomography, the fundamental equation of the PAT method may be directly inverted in relation to the function

$$\left\langle S(\mathbf{r},t) \right\rangle = \int_V S(\mathbf{r}_1,t) P(\mathbf{r}_1,t;\mathbf{r},t)\, d^3 r_1 , \tag{14}$$

viz. the function blurred due to averaging over the spatial distribution of photons, which form the signal measured by the receiver at the moment t. It is clear that the underlying function $S(\mathbf{r},t)$ can not be exactly restored, as the averaging function $P(\mathbf{r}_1,t;\mathbf{r},t)$ is variable and depends on the source-receiver positions and the intermediate time instant t. Moreover, as it follows from expression (7), $P(\mathbf{r}_1,t;\mathbf{r},t)$ is not a function of the difference $\mathbf{r}-\mathbf{r}_1$ even for the simplest geometry of the infinite space. Therefore, averaging (14) can not be expressed as convolution (9), image blurring by the PAT reconstruction procedure is spatially variant, and deconvolution deblurring may not be applied in the strict sense. The model accepted by us for image restoration is based on an assumption that the full image may be sectioned on small local regions, each of which is characterized by spatially invariant resolution. Such model results from a particularity of the PAT method and based on knowledge of *a priori* information about the character of the spatial distributions being restored. Indeed, by the PAT method blurred disturbances of the optical parameters are reconstructed. In clinical practice, when a tumor structure is detected, it may be expected that these disturbances are not random heterogeneous distributions, but they are smooth functions standing out against a zero-mean background and forming the macroinhomogeneity images. We assume that inside of local region occupied by such macroinhomogeneity two point objects located at different positions are blurred equally. Therefore, the several spatially invariant PSF is in congruence with this local region of macroinhomogeneity. Such blurring model has been validated [12, 15] and successfully used [11-15] by us for estimating the spatial resolution in a central region of an object. Thus, the convolution form (9) may be accepted for representing blurred local image and the deconvolution algorithms may be applied for its deblurring. Taking into consideration expression (7), we assume the simplest Gaussian form

$$p(\mathbf{r}) = (\sqrt{2\pi}\,\sigma)^{-3} \exp\left(-\frac{|\mathbf{r}|^2}{2\sigma^2}\right) \tag{15}$$

for the PSF used for deblurring. We will show below that the PSF kernel width σ can be estimated for different local regions of image as a function of the spatial resolution and, therefore, as a function of the macroinhomogeneity position.

2.3 The deconvolution deblurring algorithms

Digital deconvolution deblurring is the established methodology to achieve high resolution retrospectively. In this paper we consider the expectation-maximization deconvolution approach with its two realizations: the ML and LR algorithms. This approach is successfully applied for improving image clarity by optimal deterministic linear deblurring [22-24]. The standard unaccelerated LR algorithm [25, 26] is expressed by the formulae

$$f_{k+1} = f_k \cdot \left(\bar{p} \otimes \frac{\langle f \rangle}{p \otimes f_k} \right) = y(f_k), \tag{16}$$

where $\bar{p}$ is the complex conjugate of p, and $y(f_k)$ is the Lucy-Richardson function. The acceleration method implemented by us uses an additive correction factor obtained by a line search technique [18, 20]:

$$f_{k+l} = f_k + l \cdot [y(f_k) - f_k], \tag{17}$$

where l is the estimated acceleration factor. The accelerated ML algorithm [18-21] is implemented by the same formulas, but unlike the LR algorithm the PSF is updated at each iteration as follows

$$p_{k+l} = p_k + l \cdot [x(p_k) - p_k], \text{ where } x(p_k) = p_k \cdot \left(\bar{f}_{k-1} \otimes \frac{\langle f \rangle}{p_k \otimes f_k} \right). \tag{18}$$

The shortcoming of the expectation-maximization approach is in its noise and edge effects [27]. As the iteration process goes on, some disturbing artifacts become evident. At the same time, sharp transitions or edges in the image being restored become greatly accentuated with substantial overshoots, much like the well-known Gibbs phenomenon. The noise effect appears as large peaks and valleys seemingly randomly distributed throughout the image. The edge effect appears as ridges and valleys that follow edges in the underlying image. To escape these effects, the number of iterations for the restoration procedure should be optimized.

3. The restoration algorithm as a sequence of stages

After theoretical consideration presented above the restoration algorithm for PAT reconstruction deblurring can be detailed as the following sequence of stages:

- ***Stage 1.*** *Reconstruct the blurred image by the PAT method using one of algebraic techniques.*
- ***Stage 2.*** *Estimate the position of the optical macroinhomogeneity at the reconstructed image.*
- ***Stage 3.*** *Estimate the theoretical resolution for the macroinhomogeneity position calculated at stage 2 and define the kernel width s of the Gaussian point spread function.*
- ***Stage 4****: Deblur the image with the use of the iterative deconvolution algorithms for different number of iterations .*
- ***Stage 5.*** *Estimate the optimal iteration number and choose the optimal restoration result as the underlying deblurred image.*

3.1 Reconstruction of the blurred image

To reconstruct the blurred image using one of algebraic techniques, a discrete model is built up by a common way [17]. A grid of rectangular image elements or cubic volume ones (hereinafter cells) covers the reconstruction area. The value of reconstructed function $\langle S(\mathbf{r},t) \rangle$ at each j-cell is assumed to be constant and equal to S_j. Each i-PAT L_i is associated with a relative shadow g_i. If v_{ij} is the velocity of movement of the mass centre of photon distribution along the PAT L_i at the instant, when the mass centre passes through the j-cell, and A_{ij} is the length of intersection of the PAT with this cell, then the discrete model of reconstruction is described by a system of linear algebraic equations

$$\mathbf{g} = \mathbf{W} \cdot \mathbf{S}, \tag{19}$$

where $W_{ij} = (c/n_0) A_{ij} / v_{ij}$. To reverse system (19), we have chosen the QR-factorization least-squares algorithm (LSQR algorithm, [16]) oriented on strongly sparse matrixes of coefficients. The algorithm provides for the special technique to store the weighting matrix $\mathbf{W}$. This technique eliminates operations with null members in the course of calculations. It results in a significant reduction of the amount of calculations compared, for example, to well known

nonnegative least-square algorithm [28], and requires for a lesser disk space and working memory of computer. The peculiarity of realization of the LSQR algorithm is in the fact that the linear least-squares problem is stated for the augmented system

$$\overline{\mathbf{g}} = \overline{\mathbf{W}} \cdot \mathbf{S}, \tag{20}$$

where $\overline{\mathbf{g}} = \begin{bmatrix} \mathbf{g} \\ \mathbf{0} \end{bmatrix}$, $\overline{\mathbf{W}} = \begin{bmatrix} \mathbf{W} \\ l\,\mathbf{I} \end{bmatrix}$, $\mathbf{0}$ is the zero vector, l is the damping parameter, and $\mathbf{I}$ is the identity matrix. The problem is defined as follows: find the solution vector $\mathbf{S}$ that satisfies system (20) and the minimization condition for the Euclidian norm of discrepancy vector $\left\| \overline{\mathbf{g}} - \overline{\mathbf{W}}\mathbf{S} \right\| \to \min$. The LSQR algorithm is based on the bidiagonalization procedures of Golub and Kahan [29] and on the orthogonal QR-factorization using the modified flat rotation technique [16, 28]. The sequence of algorithm processing is described by Paige and Saunders [16] and does not a subject of this paper. The main difficulty of the PAT method implementation is that the statistical characteristics L_i and v_{ij} should be determined for each source-receiver pair. We have shown in [8, 9, 11] that for most object geometries, wherein a source and a receiver lie on the boundary of the object, a there-segment polygonal line can be used to approximate a curvilinear PAT. The first and the end segments of this broken line are normal to the object boundary and equal in length, and the middle segment connects their ends. The velocity of the photon distribution mass centre is inversely proportional to the distance from the object boundary when moving the centre along the outer segments of the broken PAT, and takes the stationary value when moving along the middle segment. Such approximations greatly simplify the weighting matrix calculations and considerably save the reconstruction time. Our experience [11] on the PAT method implementation using the LSQR algorithm shows that this implementation not only is very fast (computing time is approximately equal to 1 s in the case of 2D reconstruction and to half a minute in the case of 3D reconstruction), but it allows the blurred images of good quality without visible noise to be reconstructed.

3.2 Estimation of the macroinhomogeneity position

To estimate boundaries of the macroinhomogeneity and coordinates of its centre, unknown under the real circumstances, image segmentation methods well developed in recent time can be applied. In our case, when it is enough to determine the macroinhomogeneity position highly approximately, one of region-based methods [30-32] may be chosen. These methods rely on the homogeneity of spatially localized features such as gray level intensity, texture and other cell statistics. Homogeneity does not necessary mean identical cell values within a particular region, rather it means that the variation within a region is of a smaller extent then that between regions. In the present paper an approximate approach to estimate the boundaries and the centre coordinates is used. We assume a sphere (a circle in the 2D case) with identical cell values to simulate the macroinhomogeneity blurred after reconstruction. Let the unknown dummy image $\hat{f}$ is characterized by the radius-vector of the sphere centre $\mathbf{r}_m$, the sphere radius R_m, and the value of sphere cells S_m. Then the problem of macroinhomogeneity position estimation is reduced to determination of a set of parameters $\mathbf{r}_m^{opt}, R_m^{opt}, S_m^{opt}$, which minimizes the objective function

$$y = \mathrm{RMSE}\left(\hat{f}\left(\mathbf{r}_m, R_m, S_m\right), \langle f \rangle \right), \tag{21}$$

where $\mathrm{RMSE}\left(A, B\right)$ is a root-mean-square-error function defined as follows

$$\mathrm{RMSE}\left(A, B\right) = \sqrt{\frac{1}{N}\sum_j^N \left(A_j - B_j\right)^2}, \tag{22}$$

for two images $A \equiv \left\{A_j\right\}_1^N$ and $B \equiv \left\{B_j\right\}_1^N$. Here N is the number of image cells. The solution of the fifth- or fourth-order minimization problem formulated above by handling all values of parameters being optimized is impeded due to the considerable increase of computing time. To simplify the problem, we assume that the global minimum of the

objective function y is a singular minimum under the optimization over the centre coordinates that are defined by the radius-vector $\mathbf{r}_m$. In this case the set of the optimal parameters can be found pretty quickly with the use of well-known methods for the determination of the extremum of a function with a few variables, as it is not required to calculate the function y for all values of parameters. To minimize function (21) over the centre coordinates, we apply the approach as follows. Let the coordinates of some initial point $\mathbf{r}_m^0$ lying inside of the macroinhomogeneity region are known. If the sphere radius is more better than the extension of local noise at the blurred image, the local minimum of y inside of any locality of the point $\mathbf{r}_m^0$ will be run into a new point $\mathbf{r}_m^1$ that is closer to the point of the global maximum $\mathbf{r}_m^{opt}$ than the initial one. Thus, for estimating the coordinates of the macroinhomogeneity centre, the fast iterative algorithm based on the consequent determination of local minimums inside of the point localities may be used.

3.2 Definition of the kernel width of the Gaussian PSF

As it well known, if the linear filter invariant to the spatial shift simulates a visualization system, the PSF may be used to estimate the image resolution. Commonly they take the full width at half maximum (FWHM) of the PSF for resolution estimation. If the PSF has Gaussian form (15), the kernel width s may be found as follows

$$\frac{1}{2} = \exp\left(-\frac{(\Delta/2)^2}{2s^2}\right) \Rightarrow \quad s = \frac{\Delta}{2\sqrt{2\ln 2}}, \tag{23}$$

where Δ is the FWHM estimating the spatial resolution. Laying account with expression (8), for a spherical or circular scattering object with diameter d we can write the following simple formulae

$$s(r) = \sqrt{\frac{3D_0 c}{2\ln 2 \cdot n_0}\left(t - \frac{dn_0}{c}\right)\left(\frac{1}{4} - \frac{r^2}{d^2}\right)}, \tag{24}$$

where r is the macroinhomogeneity displacement from the object centre. As the value r is estimated at stage 2, formulae (24) allows the PSF kernel width to be calculated for any local region of the object, containing the macroinhomogeneity.

3.4 Image deblurring implementation and estimation of the optimal iteration number

In this paper, we use the Matlab functions "*deconvblind*(·)" and "*deconvlucy*(·)" that realize the ML and LR algorithms, respectively, shortly described by us in section 2.3. Both functions deconvolve the blurred image returning the restored image on each iteration of the iterative process. The iteration number, for which the restored image is outputted, is specified by user. We can restore the images for different number of iterations and then compare the obtained results over the double criterion of resolution maximum and artifact level minimum. Such approach based on visual analysis of restored images is available in clinical circumstances, when the underlying image f is unknown. If the experiment with phantoms is conducted, we have a reason to apply a quantitative criterion for estimating the optimal iteration number. In [33] the authors suggest to use the following blurring residual for measuring the image quality change after deblurring a blurred image:

$$b_k = \frac{\mathrm{RMSE}(f_k, f)}{\mathrm{RMSE}(\langle f \rangle, f)}\%. \tag{25}$$

At the first iterations the restored image looks to the underlying one and the blurring residual b_k falls away. As the iteration process goes on, the noise and edge effects intensify, and the factor b_k begins to increase. Thus, the blurring residual has a minimum that corresponds to the optimal iteration number.

4. Results and analysis

To demonstrate the effect of improving the spatial resolution of diffuse optical images reconstructed by the PAT method, a numerical experiment was conducted, wherein cross-sections of cylindrical strongly scattering objects were reconstructed. The diameter of objects was equal to 6.8 cm. The refraction index, coefficients of diffusion and absorption of the objects were equal to 1.58, 0.0636 cm and 0.042 cm^{-1}, correspondingly. We considered two sets of phantoms. Each phantom of the first set contained a cylindrical absorbing inhomogeneity with the diameter equal to 1 cm (absorption coefficient was equal to 0.17 cm^{-1}). In one of the cases, the inhomogeneity was located in the center of the object, in the two others it was displaced from the center by 1.25 and 2.5 cm, correspondingly. The second set of phantoms was designated to measure the modulation transfer function (MTF) that is commonly used for spatial resolution estimation. We used four cylindrical strongly scattering objects, each containing two cylindrical absorbing inhomogeneities equal in diameter. The diameter and optical parameters of these objects, as well as the absorption coefficient of inhomogeneities, were identical to those for the phantoms of the first set. The distance between inhomogeneities was equal to their diameter. Diameters of inhomogeneities of different objects were equal to 1.4, 1.2, 1.0, and 0.8 cm. Sources (32) and receivers (32) were installed along the perimeter of the objects at equal step angles (11.25^0). In so doing, the angular distance between the nearest-neighbor source and receiver constituted 5.625^0. The relative shadows caused by the absorbing inhomogeneity were simulated via numerical solution of time-dependent diffusion equation for the instantaneous point source (the case of time-domain measurement technique) with the use of FEM method. Reconstruction of cross-sections for each phantom with the use of the LSQR algorithm was realized onto rectangular grid 44*44. The reconstruction results for phantoms of the first set are presented in figure 2 as gray level images in comparison with the results of deblurring for the optimal iteration number. The blurred images are given on the left. The central column of images corresponds to the restoration results obtained with the use of the ML algorithm. And the images deblurred by the LR algorithm are presented in figure 2 on the right. The upper images correspond to the object with the central inhomogeneity, the central row of images — to the object with the inhomogeneity displaced from the center by 1.25 cm and the bottom ones — to the object with the inhomogeneity displaced by 2.5 cm. White points in the images show the object boundaries that are known *a priori*. The coordinate axes are graduated in centimeters and the intensity scale — in reverse centimeters. The blurred reconstructions and the results of their restoration for phantoms of the second set are given as surface plots in figure 3. Like figure 2, the blurred images are given on the left. The ML restorations are shown in the centre, and the LR ones – on the right of figure 3. The sequence of image triplets from top to bottom corresponds to a scale of inhomogeneity diameters from 1.4 to 0.8 cm. The intensity values are separately normalized for each image and shown on a percent scale (vertical axes of the plots). Before all images were restored the inhomogeneity positions were estimated at the blurred images of phantoms of the first set. The results of these estimations checked with real positions accurate within 2 mm. The PSF kernel width was defined under formulae (24) for each estimated value of the inhomogeneity displacement from the phantom centre. The results of image restoration were obtained with the use of both deblurring algorithms for different number of iterations. Some of the restoration results for the image with the central inhomogeneity are presented in figure 4. The upper images correspond to the restorations by the ML algorithm and the bottom ones – to the LR restorations. The pairs of images from left to right are deblurred for iteration number equal to 2, 5, and 10, respectively. One can see that the right images are not of good quality. There is a distortion of the inhomogeneity profile in the case of the ML restoration. And the noise is on the increase in the case of LR one. It means that the optimal iteration number is less than 10 in both cases. To estimate the optimal iteration number we used the blurring residual given by expression (25). The estimation results for images with the central inhomogeneity equaled to 5 and 8 iterations in the cases of ML and LR algorithms, correspondingly. These values were also accepted as the optimal iteration numbers for restoration of all blurred images presented in figures 2 and 3. Inhomogeneity position estimations did not carry out for images of the objects with two inhomogeneities and *a priori* information was used to define the PSF kernel width. On the base of the profile of each image of figure 3 the modulation transfer coefficient (MTC) was determined as a relative depth of a dish between two peaks. The numerical results of MTC estimations are also provided in figure 3. Discrete values of spatial frequency were put in conformity with diameters of inhomogeneities. To estimate the MTF, a dependence of the MTC on spatial frequency was accepted (figure 5). From figure 5 it is visible, that with contrast of not less than 20% the spatial frequencies of not more than 0.5, 0.58 and 0.64 cycles/cm can be reproduced on images blurred due to reconstruction and those restored by ML and LR algorithms, correspondingly. It means that the inhomogeneities with linear sizes of 1.0, 0.87 and 0.78 cm can be resolved on the coincident images. Thus, the gain in spatial resolution achieves ~13% in the case of the ML restorations and ~22% – in the case of the RL ones. The latest estimation seems to be identical to the result obtained with the use of the Vainberg or Vainberg-Butterworth backprojection algorithm [12-15]. Therefore, to

improve the resolution of the PAT reconstructions, not only special filtration of shadows, but post-reconstruction restoration may be successfully used.

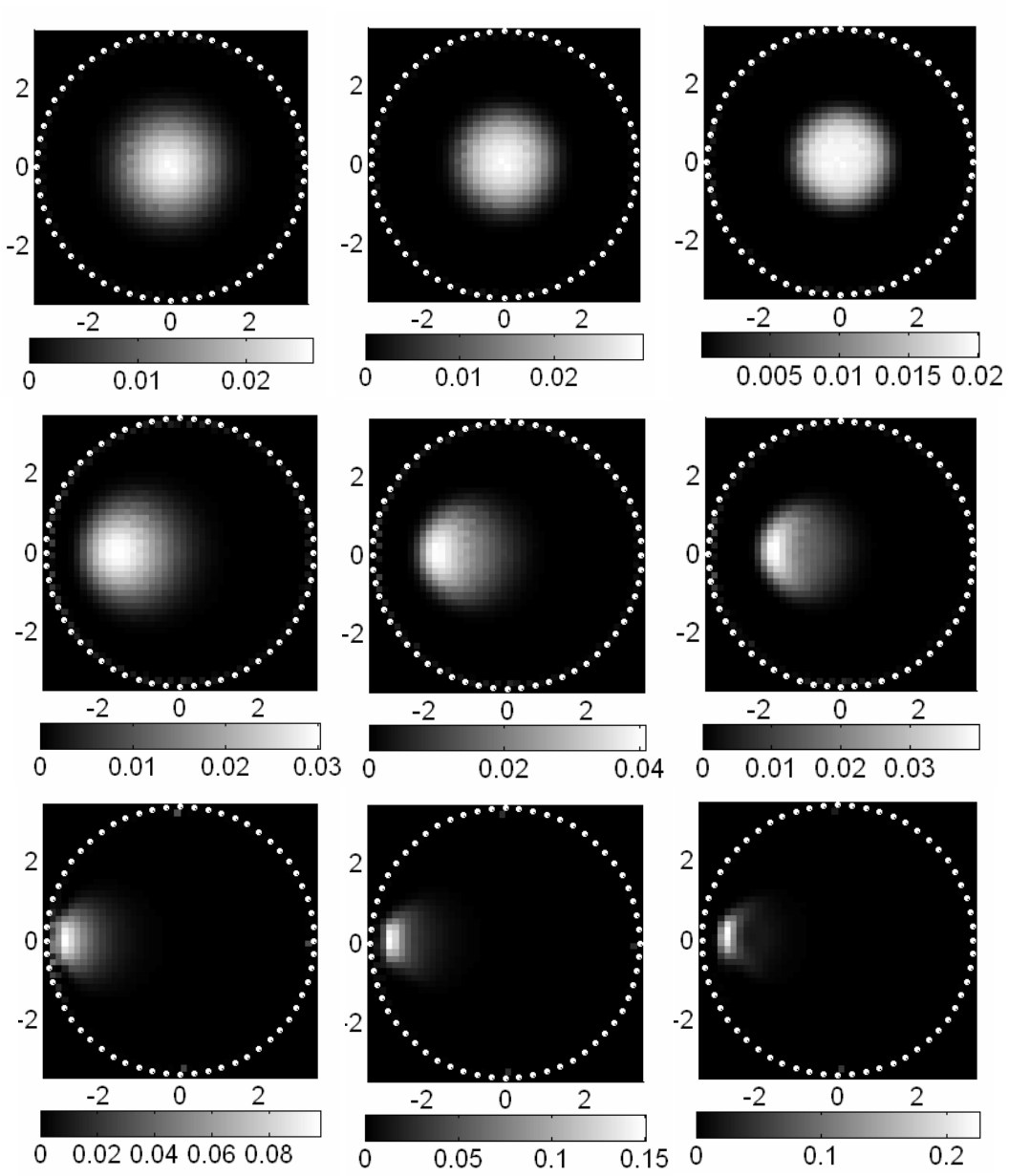

Figure 2. The results of reconstruction by the LSQR algorithm – the blurred images (left) and the results of debluring: with the use of the ML algorithm (centre) and the LR algorithm (right) for phantoms of the first set.

However, figure 2 (see the central row of images) shows that, as the inhomogeneity is shifted from the object center, its deblurred image become to jump. Especially it applies to the LR restoration, wherein the circle looks like a crescent. The form distortions are practically inappreciable on the bottom images of figure 2, since the spatial resolution is improved, when the object boundary is approached. Thus, the spatially invariant blurring model accepted in the present paper seems to be not completely effective for deblurring the image regions remote well away from the centre and the boundary.

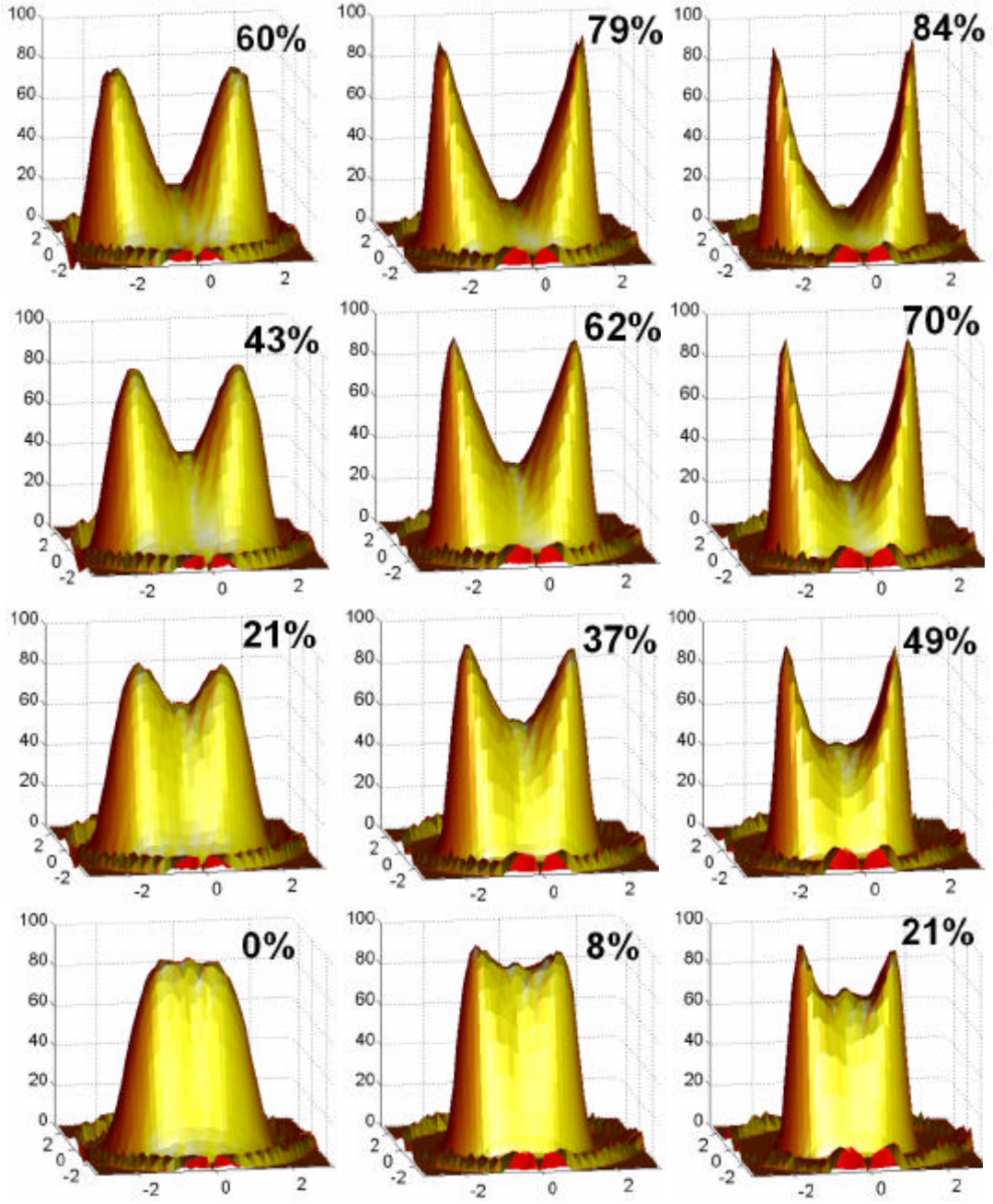

Figure 3. The results of reconstruction by the LSQR algorithm – the blurred images (left) and the results of debluring: with the use of the ML algorithm (centre) and the LR algorithm (right) for phantoms of the second set.

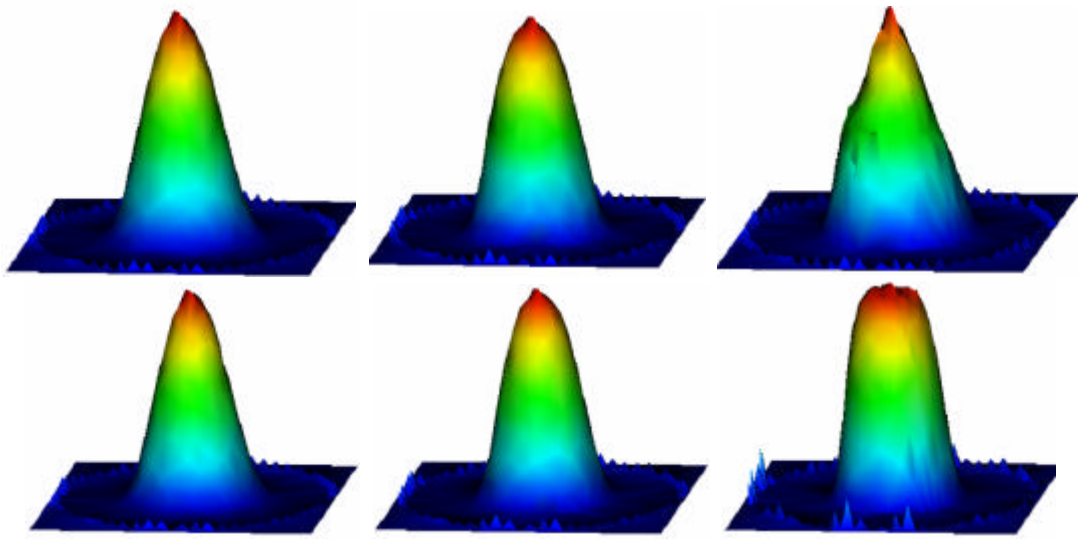

Figure 4. The results of debluring with the use of the ML algorithm (upper) and the LR algorithm (bottom) for different number of iterations (2, 5, and 10).

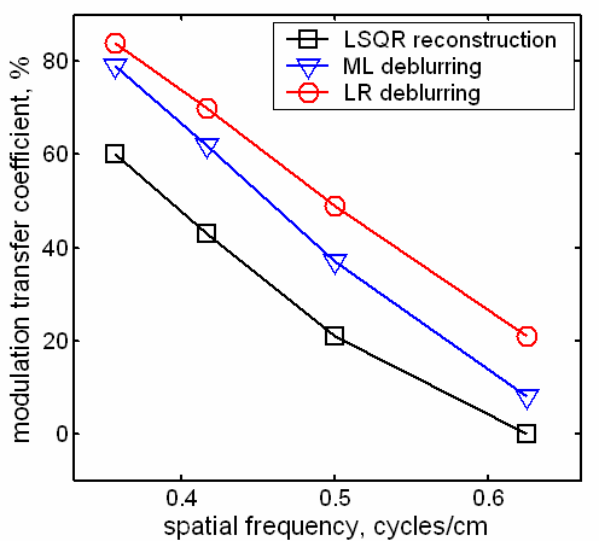

Figure 5. MTF estimations for blurred and restored images.

6. Conclusion

In this paper we have examinated the possibility of the application of deconvolution deblurring to improve the spatial resolution of diffuse optical images reconstructed by the new photon average trajectories method. The spatially invariant blurring model was developed to restore local images of macroinhomogeneities imbedded in a homogeneous strongly scattering object. To estimate the underlying point spread function describing the image degradation, we have assumed a simple Gaussian form with the kernel width that depends on the macroinhomogeneity displacement from the object centre. To study the efficiency of the blurring model proposed, two algorithms based on the expectation-maximization approach to restoration were implemented. Those are the maximum likelihood and Lucy-Richardson algorithms. We have conducted a numerical experiment on cross-sectional reconstruction and restoration of cylindrical phantoms with cylindrical absorbing inhomogeneities. To reconstruct the blurred images under simulated time-domain measurements, the well-known QR-factorization least-squares algorithm was used. The analysis of the restoration results presented shows that the deconvolution deblurring algorithms are efficient for high-resolution restoring the

diffuse optical images, when the macroinhomogeneity is located close to the centre or the boundary of the object. So, the Lucy-Richardson algorithm allows the 22%-gain in spatial resolution to be obtained. If the macroinhomogeneity is remote well away from the centre or the boundary of the object, the form distortions become to be visible on the restored images. In the future more examples, in particular, for multi-target objects should be considered to test the limits of a spatially invariant blurring model. The development of a spatially variant model is also the subject of our short-term interest.

Acknowledgments

The authors would like to thank O V Lyamtsev with the Interact Devices, Folsom, USA, L M Yavorskaya, I I Kutuzov, O V Golubkina, G B Mordvinov, K B Domrachev with the Russian Federal Nuclear Centre, Snezhinsk, Russia, and L N Soms, O V Kravtsenyuk, A G Murzin, A G Kalintsev with the Research Institute for Laser Physics, St.-Petersburg, Russia for fruitful and helpful discussions during the research preparation.

References

1. Arridge S R 1999 Optical tomography in medical imaging *Inverse Problems* **15** R41–R93
2. Yodh A and Chance B 1995 Spectroscopy and imaging with diffusing light *Phys. Today* **48** 34-40
3. Hielscher A H, Klose A D and Hanson K M 1999 Gradient-based iterative image reconstruction scheme for timeresolved optical tomography *IEEE Trans. Med. Imaging* **18** 262–71
4. Lyubimov V V 1995 The physical foundation of the strongly scattering media laser tomography *Proc. SPIE* **2769** 107–10
5. Lyubimov V V 1996 Optical tomography of highly scattering media using first transmitted photons of ultrashort pulses *Opt. Spectrosc.* **80** 687–90
6. Lyubimov V V, Kravtsenyuk O V, Mironov E P and Murzin A G 1997 On the calculation of shadows induced by macroinhomogeneities located inside a strongly scattered objects using the integral over the average photon path *Proc. SPIE* **3194** 409–16
7. Lyubimov V V 1999 On the spatial resolution of optical tomography of strongly scattering media with the use of the directly passing photons *Opt. Spectrosc.* **86** 251–2
8. Volkonskii V B, Kravtsenyuk O V, Lyubimov V V, Mironov E P and Murzin A G 1999 The use of the statistical characteristics of the photons trajectories for the tomographic studies of the optical macroheterogeneities in strongly scattering objects *Opt. Spectrosc.* **86** 253–60
9. Kravtsenyuk O V and Lyubimov V V 2000 Specific features of statistical characteristics of photon trajectories in a strongly scattering medium near an object surface *Opt. Spectrosc.* **88** 608–14
10. Kravtsenyuk O V and Lyubimov V V 2000 Application of the method of smooth perturbations to the solution of problems of optical tomography of strongly scattering objects containing absorbing macroinhomogeneities *Opt. Spectrosc.* **89** 107–12
11. Lyubimov V V, Kalintsev A G, Konovalov A B, Lyamtsev O V, Kravtsenyuk O V, Murzin A G, Golubkina O V, Mordvinov G B, Soms L N and Yavorskaya L M 2002 Application of photon average trajectories method to real-time reconstruction of tissue inhomogeneities in diffuse optical tomography of strongly scattering media *Phys. Med. Biol.* **47** 2109-28
12. Lyubimov V V, Konovalov A B, Kutuzov I I, Kravtsenyuk O V, Kalintsev A G, Murzin A G, Golubkina O V, Soms L N and Yavorskaya L M 2002 Influence of fast reconstruction algorithms on spatial resolution of optical diffuse tomography by photon average trajectories method *Proc. SPIE* **4707** 53–9
13. Konovalov A B, Lyubimov V V, Kutuzov I I, Kravtsenyuk O V, Murzin A G, Mordvinov G B, Soms L N and Yavorskaya L M 2002 Application of integral transform algorithms to high-resolution reconstruction of tissue inhomogeneities in medical diffuse optical tomography *Proc. SPIE* **4916** 9–21
14. Konovalov A B, Lyubimov V V, Kutuzov I I, Kravtsenyuk O V, Murzin A G, Mordvinov G B, Soms L N and Yavorskaya L M 2003 Application of the transform algorithms to high-resolution image reconstruction in optical diffusion tomography of strongly scattering media *J. Electron. Imaging* **12(4)** 602–12
15. Lyubimov V V, Kravtsenyuk O V, Kalintsev A G, Murzin A G, Soms L N, Konovalov A B, Kutuzov I I, Golubkina O V and Yavorskaya L M 2003 The possibility of increasing the spatial resolution in diffusion optical tomography *J. Opt. Technol.* **70** 715–20
16. Paige C C and Saunders M A 1982 LSQR: An algorithm for sparse linear equations and sparse least squares *ACM Trans. on Math. Softw.* **8** 43–71

17. Censor Y 1983 Finite series-expansion reconstruction methods *Proc. IEEE* **71** 409–19
18. Biggs D S C and Andrews M 1997 Acceleration of iterative image restoration algorithms *Appl. Opt.* **36** 1766–75
19. Ayers G R and Dainty J C 1988 Iterative blind deconvolution method and its applications *Opt. Lett.* **13(7)** 547–9
20. Hanisch R J, White R L and Gilliland R L 1997 Deconvolutions of Hubble Space Telescope images and spectra *Deconvolution of Images and Spectra* ed P A Jansson (2nd ed Academic Press: CA) pp 310–60
21. Holmes T J, Bhattacharyya S, Cooper J A, Hanzel D, Krishnamurthi V, Lin W-C, Roysam B, Szarowski D H and Turner J N 1995 Light microscopic images reconstructed by maximum likelihood deconvolution *Handbook of biological confocal microscopy* ed J B Pawley (2nd ed Plenum Press: New York) pp 389–402
22. Csiszar I 1991 Why least squares and maximum entropy? An axiomatic approach to inference for linear inverse problems *The Annals of Statistics* **19(4)** 2032–66
23. Snyder D L, Schulz N J and O'Sullivan J A 1992 Deblurring subject to nonnegativity constraints *IEEE Trans. Signal Processing* **40(5)** 1143–50
24. Vannier M W and Wang G 1993 Spiral CT refines temporal bone imaging *Diagnostic Imag.* **15** 116–21
25. Richardson W H 1972 Bayesian-based iterative method of image restoration *J. Opt. Soc. Am.* **62** 55–9
26. Lucy L B 1974 An iterative technique for the rectification of observed distributions *Astron. J.* **79** 745–54
27. Snyder D L, Miller M I, Thomas L J and Politte D G 1987 Noise and edge artifacts in maximum-likelihood reconstructions for emission tomography *IEEE Trans. Med. Imag.* **MI-6** 228–38
28. Lawson C L and Hanson R J 1974 *Solving Least Squares Problems* (Englewood Cliffs, NJ: Prentice-Hall)
29. Golub G H and Kahan W 1965 Calculating the singular values and pseudoinverse of a matrix *SIAM J. Numer. Anal.* **2** 205-24
30. Geiger D and Yuille A 1991 A common framework for image segmentation *Int. J. Comput. Vision* **6** 227–43
31. Geman D and Geman S 1984 Stochastic relaxation, Gibbs distribution and Bayesian restoration of images *IEEE Trans. Pattern Anal. Machine Intell.* **PAMI-6** 721–41
32. Perona P and Malik J 1990 Scale-space and edge detection using anisotropic diffusion *IEEE Trans. Pattern Anal. Machine Intell.* **PAMI-12** 629–39
33. Jiang M, Wang G, Skinner M W, Rubinstein J T and Vannier M W 2003 Blind deblurring of spiral CT images *IEEE Trans. Med. Imag.* **22(7)** 837–45